Available online at www.sciencedirect.com
ScienceDirect
International Journal of Heat and Mass Transfer 50 (2007) 3862–3876
International Journal of HEAT and MASS TRANSFER
www.elsevier.com/locate/ijhmt

Saturated flow boiling heat transfer and associated bubble characteristics of FC-72 on a heated micro-pin-finned silicon chip

Y.M. Lie [a], J.H. Ke [a], W.R. Chang [c], T.C. Cheng [b], T.F. Lin [a,*]

[a] *Department of Mechanical Engineering, National Chaio Tung University, Hsinchu, Taiwan, ROC*
[b] *National Nano Device Laboratories, Industrial Technology Research Institute, Hsinchu, Taiwan, ROC*
[c] *Energy and Resources Laboratories, Industrial Technology Research Institute, Hsinchu, Taiwan, ROC*

Received 22 December 2005; received in revised form 3 February 2007
Available online 11 April 2007

Abstract

An experiment is carried out here to investigate flow boiling heat transfer and associated bubble characteristics of FC-72 on a heated micro-pin-finned silicon chip flush-mounted in the bottom of a horizontal rectangular channel. Besides, three different micro-structures of the chip surface are examined, namely, the smooth, pin-finned 200 and pin-finned 100 surfaces. The pin-finned 200 and 100 surfaces, respectively, contain micro-pin-fins of size 200 μm × 200 μm × 70 μm (width × length × height) and 100 μm × 100 μm × 70 μm. The pitch of the fins is equal to the fin width for both surfaces. The effects of the FC-72 mass flux, imposed heat flux, and surface micro-structures of the silicon chip on the FC-72 saturated flow boiling characteristics are examined in detail. The experimental data show that an increase in the FC-72 mass flux causes a delay in the boiling incipience. However, the flow boiling heat transfer coefficient is not affected by the coolant mass flux. But adding the micro-pin-fin structures to the chip surfaces can effectively enhance the single-phase convection and flow boiling heat transfer. Moreover, the mean bubble departure diameter and active nucleation site density are reduced for a rise in the FC-72 mass flux. A higher coolant mass flux results in a higher mean bubble departure frequency. Furthermore, larger bubble departure diameter, higher bubble departure frequency, and higher active nucleation site density are observed at a higher imposed heat flux. We also note that adding the micro-pin-fins to the chips decrease the bubble departure diameter and increase the bubble departure frequency. However, the departing bubbles are larger for the pin-finned 100 surface than the pin-finned 200 surface but the bubble departure frequency exhibits an opposite trend. Finally, empirical equations to correlate the present data for the FC-72 single-phase liquid convection and saturated flow boiling heat transfer coefficients and for the bubble characteristics are provided.
© 2007 Elsevier Ltd. All rights reserved.

1. Introduction

The recent quick development of the IC (Integrated Circuits) technology significantly reduces the size of the electronic equipments and substantially increases the density of the power dissipation in the equipments. It is well known that the heat removal methods based on gas cooling are not sufficiently effective for the high-emission heat components. The direct liquid cooling is better. Moreover, flow boiling is one of the most effective methods because the high latent heat involved in the process. The dielectric coolant FC-72 is appropriate for the electronics cooling. Up to the present, the bubble characteristics associated with the cooling of electronic equipments by flow boiling of dielectric liquids remain poorly understood. The situation is even worse for flow boiling on some enhanced surfaces. Hence the relation between the bubble behaviors and heat transfer performance can not be delineated.

In the following the literature relevant to the present study is reviewed. Mudawar and his colleagues [1,2] experimentally examined subcooled flow boiling of FC-72 over

* Corresponding author. Tel.: +886 35 712121 55118; fax: +886 35 726440.
E-mail address: tflin@mail.nctu.edu.tw (T.F. Lin).

0017-9310/$ - see front matter © 2007 Elsevier Ltd. All rights reserved.
doi:10.1016/j.ijheatmasstransfer.2007.02.010

Nomenclature

A_{chip}	surface area of a bare chip (m^2)
A_f	surface area of a single fin (m^2)
Bo	Boiling number, $Bo = \frac{q}{G \cdot i_{fg}}$, dimensionless
B_f	fin height (m)
c_p	specific heat (J/kg °C)
$d_p, \overline{d_p}$	mean dimensional and dimensionless bubble departure diameter (m)
D_h	hydraulic diameter of rectangular-channel (m)
E	enhancement factor
$f, \bar{f}$	mean dimensional and dimensionless bubble departure frequency (s^{-1})
F_{sp}, $F_{d,sat}$	pin-fin factors for the effects of fin geometries, dimensionless
Fr_l	Froude number, $Fr_l = \frac{G^2}{\rho_l^2 \cdot g \cdot D_h}$, dimensionless
g	acceleration due to gravity (m/s^2)
G	mass flux (kg/m^2 s)
h_l, h_r	single and two-phase heat transfer coefficients (W/m^2 K)
H	height (m)
i_{lv}	enthalpy of vaporization (J/kg K)
I	measured current from DC power supply (A)
k	thermal conductivity (W/m K)
L	length (m)
N	number of micro-pin-fins
N_{ac}	mean active nucleation site density (n/m^2)
N_{conf}	Confinement number, $N_{conf} = \frac{(\sigma/g \cdot \Delta\rho)^{0.5}}{D_h}$, dimensionless
Nu_l	Nusselt number for liquid convection, $Nu_l = \frac{h_l \cdot L}{k_l}$, dimensionless
P	system pressure (kPa)
Pr	liquid Prandtl number, $Pr = \frac{\mu_l \cdot c_p}{k_l}$, dimensionless
Q_e, Q_t	effective and total heat transfer rates (W)
q''	average effective imposed heat flux (W/m^2)
$R_{c,h}$	resistances of the cooper and mica plates
Re_l	liquid Reynolds number, $Re_l = \frac{G \cdot D_h}{\mu_l}$, dimensionless
S_f	fin space between two adjacent fins (m)
T_{chip}, T'_{chip}	temperatures at the upper and lower surfaces of chip (K)
T_{heater}	temperature of the heater surface (K)
T_{in}	liquid temperature at test section inlet (K)
T_{sat}	saturated temperature of FC-72 (K)
V	measured voltage from DC power supply (V)
V_b	volume of a mean departing volume (m^3)
W_f	width of a fin (m)

Greek symbols

$\Delta T_{c,h}$	temperature difference ($T_{heater} - T'_{chip}$) (K)
ΔT_{sat}	wall superheat, ($T_{chip} - T_{sat}$)
$\Delta\rho$	density difference ($\rho_l - \rho_v$) (kg/m^3)
ε	relative heat loss, dimensionless
μ_l	dynamic viscosity (N s/m^2)
ρ_l, ρ_v	liquid and vapor densities (kg/m^3)
σ	surface tension (N/m)

flush-mounted heat sources for the flow velocity ranging from 13 to 400 cm/s. They found that the heat transfer coefficient in the single-phase region varied linearly with the flow velocity and the boiling incipience was delayed for a higher flow velocity. Similar experiments were conducted by Heindel et al. [3] also for FC-72 and they noted that at increasing velocity the heat flux increased but the temperature overshoot at onset of nucleate boiling reduced. In the fully developed boiling, the velocity exhibited little effect on the boiling curves, which was also supported by McGills et al. [4]. On the other hand, a higher liquid subcooling resulted in a smaller temperature overshoot at ONB. In vertical channel flow boiling experiments for FC-72, Tso et al. [5] found that the temperature of the chip surface decreased with the increases in the flow velocity and liquid subcooling in the partial boiling region. While in the fully-developed boiling region both the flow velocity and subcooling temperature had little effects on the chip surface temperature. The temperature of the chip surface for the flush-mounted chips was lower than the protruded chips in the partial boiling region, but they were nearly equal in the fully developed boiling region. Samant and Simon [6] analyzed the heat transfer from a small region to refrigerants R-113 and FC-72 and noted that as the flow velocity and subcooling temperature increased, the temperature excursion and boiling hysteresis appeared to decrease.

Ma and Chung [7] investigated bubble dynamics in reduced gravity flow boiling of FC-72 over a thin gold film semi-transparent heater. The bubble departure size was found to be bigger in the micro-gravity than environment. At increasing flow rate, the bubble departure time and departure size decreased. This was also observed by Situ et al. [8] later. Besides, they also noted that the bubble growth rate dropped sharply after lift-off. In addition, Yin et al. [9] examined the subcooled flow boiling of R-134a in an annular duct and found that both the bubble departure size and frequency reduced at increasing liquid subcooling. Experiments conducted by Bang et al. [10] and Chang et al. [11] for R-134a and water focused on the behavior of near-wall bubbles in subcooled flow boiling. They identified four different two-phase flow patterns including the discrete attached bubbles, sliding bubbles, small coalesced bubbles and large coalesced bubbles or vapor clots at increasing heat flux. For the higher mass flux of the flow, the coalesced bubbles were smaller. Bang et al. [12] further noticed the presence of the R-134a vapor remants below the discrete bubbles and coalesced bubbles, and the presence of an interleaved liquid layer between the vapor remants and bubbles. Besides, the bubble layer could

be divided into two types, a near-wall bubble layer dominated by small bubbles and a following bubble layer prevailed by large coalesced bubbles. Using digital imaging and analyzing techniques, Maurus et al. [13] examined the bubble characteristics and local void fraction in subcooling flow boiling. The bubble population was noted to increase with the heat flux and the bubble density reduced drastically at increasing mass flux. Besides, the bubble size increased at increasing heat flux and decreasing mass flux. In a continuing study [14] they further showed that the effects of the heat flux and mass flux on the bubble size distribution were weak for small bubbles but became more pronounced for bigger bubbles. The total bubble life time, the remaining lifetime after the detachment process and the waiting time between two bubble cycles decreased significantly as the mass flux increased. Moreover, they pointed out that the bubble behavior was dominated by the temperature of the thermal boundary layer and the turbulence intensity due to the heat transport in the liquid near the interface. On the other hand, in vertical upflow and downflow boiling Thorncroft et al. [15] found that the bubble growth rate and departure diameter increased with the wall superheat but decreased with increasing mass flux.

Flow boiling of FC-72 over microstud, microgroove, and cylindrical micro pin-fin enhanced surfaces flush-mounted on a vertical rectangular-channel wall was examined by Maddox and Mudawar [16,17]. The surface micro-structures were found to significantly enhance the heat transfer performance and reduce the boiling hysteresis. Heat transfer in pool boiling of FC-72 on silicon chips with the surface micro-structures of micro-pin-fins was recently investigated by Honda et al. [18,19]. They found that both the nucleate boiling heat transfer and the critical heat flux were effectively enhanced by the micro-pin-fins. The boiling phenomena observed revealed that a small amount of vapor was left within the gap between the pin-fins when a growing bubble left the surface. On the other hand, Honda and Wei [20] conducted a critical review on the boiling heat transfer enhanced by the surface-structures. They indicated that all the surface micro-structures including the micro-roughness, micro-reentrant, and micro-porous structures were helpful in reducing the boiling incipience superheat. Surface cavities were effective in increasing critical heat flux and in enhancing nucleate boiling. Generally, the micro-pin-fins were most effective in augmenting CHF and micro-porous structures were most effective in enhancing nucleate boiling heat transfer. Recently, Ramaswamy et al. [21] examined the effects of varying geometrical parameters on boiling from microfabricated enhanced structures. They indicated that increasing pore size caused higher heat dissipation and the pore pitch had more significant effect on the heat transfer performance. Finally, heat transfer from the microporous finned surface was found to have better performance than the plain finned surface [22].

The above literature review clearly indicates that the pool boiling heat transfer from micro-structured surface and the associated bubble dynamics have received some attention. But heat transfer and bubble characteristics in flow boiling of dielectric coolants on micro-structured surfaces remain largely unexplored. In this study an experiment is carried out to investigate the FC-72 flow boiling on a single silicon chip with micro-pin-fins on its surface. The chip is flush-mounted on the bottom of a horizontal rectangular channel.

2. Experimental apparatus and procedures

The experimental system established in the present study, schematically depicted in Fig. 1, consists of a degassing unit, a coolant loop, a hot-water loop, and a cold-water loop. They are described in the following.

2.1. Degassing unit

Because air or non-condensable gas dissolved in the coolant FC-72 can significantly affect the heat transfer performance and nucleate boiling phenomena, we must degas the coolant before beginning the experiments. The degassing unit is a 8-liter tank with an electric-heated patch in it to heat the coolant to its boiling point and the coolant begins to evaporate. The air and non-condensable gas and a little amount of the coolant vapor can be removed from the released valve on the top of the tank. Besides, a pressure transducer and a thermocouple are equipped in the tank to measure the pressure and temperature of FC-72, respectively.

2.2. Coolant loop

After degassing FC-72, we can remove the non-condensable gases possibly existing in the coolant loop by using a vacuum pump and then fill FC-72 into the loop. The coolant loop consists of a variable-speed magnetic micro-pump, a filter, a volume flow meter, a pre-heater, a test section including the inlet and outlet sections, a condenser, and a receiver. The coolant flow rate is mainly controlled by an AC motor and can be further adjusted by regulating a bypass valve. The coolant FC-72 at the outlet of the magnetic micro-pump must be kept subcooled to avoid any vapor flow through the volume flow meter. Finally, a vapor–liquid mixture is generated in the test section when the coolant moves over the heated silicon chip. The vapor flow leaving the test section is re-liquefied by the condenser in the cold-water loop. After leaving the condenser, the liquid FC-72 flows back to the receiver. An accumulator is connected to a high-pressure nitrogen tank to dampen the fluctuations of the coolant flow rate and pressure. The filter is used to filter the impurities and non-condensable gas possibly existing in the loop. Varying the temperature and flow rate of the hot-water flowing through the pre-heater allows us to control the pressure of the coolant loop. Two absolute pressure transducers are installed at the inlet and outlet of the test section with a resolution up to ± 2 kPa. All the coolant and water temperatures are mea-

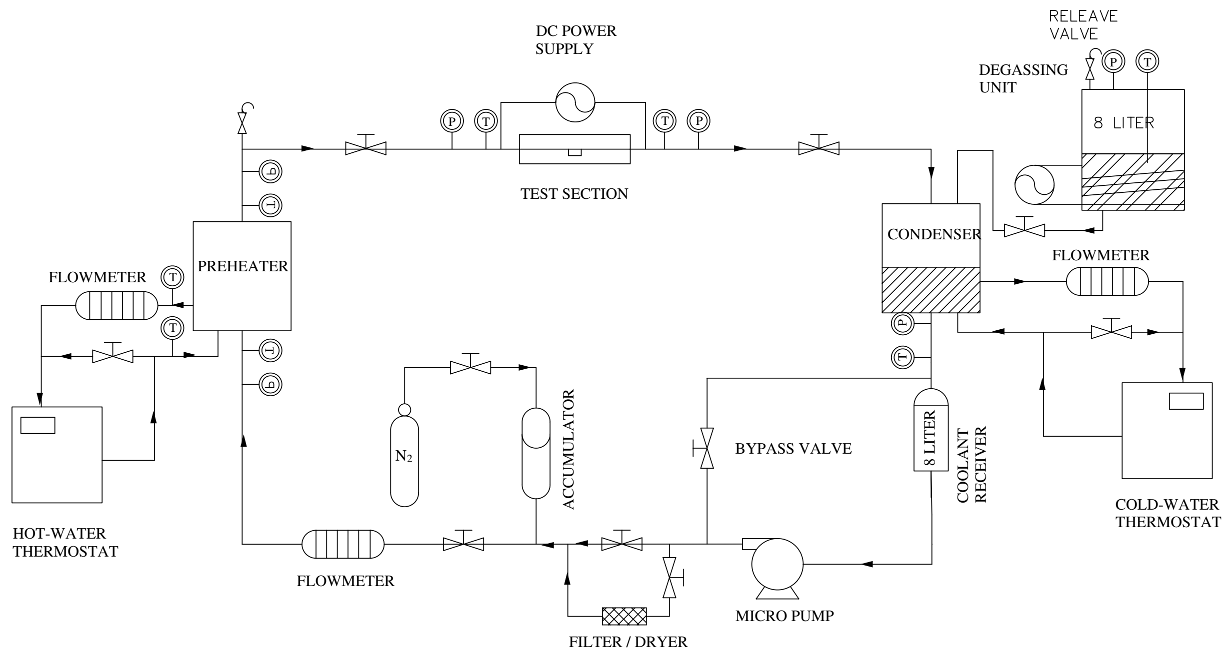

Fig. 1. Schematic diagram of experimental apparatus.

sured by copper-constantan thermocouples (T-type) with a calibrated accuracy of ± 0.2 °C.

2.3. Test section

The test section mainly contains a silicon chip flush-mounted on the channel bottom. The flow-channel consists of a gradually converging inlet section, the main test section, and a gradually diverging exit section. They are all made of stainless steel plate. The installation of the inlet and exit sections avoids the sudden change in the cross section of the channel. The test section is a rectangular channel of 20 mm in width, 5 mm in height, and 150 mm in length. The chip is mounted around the geometric center of the bottom plate of the test section. An observational window is installed on the upper lid of the test section right above the chip. The temperature and pressure of the FC-72 flow at the inlet and exit of the test section are measured by calibrated thermocouples and pressure transducers. The silicon chip module schematically shown in Fig. 2 includes a hollow cylindrical Teflon block, a cylindrical Teflon bolt, a silicon chip, a copper plate, two pieces of mica, a Teflon plate, and an electric-heater. To reduce the thermal contact resistance, thermal conducting grease is filled into the gaps between all the adjacent plates. The surface area of the silicon chip is 10 mm × 10 mm and the chip is heated by passing DC current through the electric-heater. Besides, three thermocouples are fixed at the back surface of the silicon chip to estimate the surface temperature of the silicon chip and another thermocouple is fixed at the upper surface of the electric-heater to measure its surface temperature. The square micro-pin-fins on the silicon chip are fabricated by the semiconductor manufacturing technique. Two surface micro-structures in the form of square micro-pin-fins are manufactured on the silicon chips and each individual fin has the same size of 200 μm × 200 μm × 70 μm for the pin-finned 200 surface and 100 μm × 100 μm × 70 μm for the pin-finned 100 surface. The space between the two adjacent fins (the fin pitch) is about equal to the fin width and the detailed photographs of the arrays of selected micro-

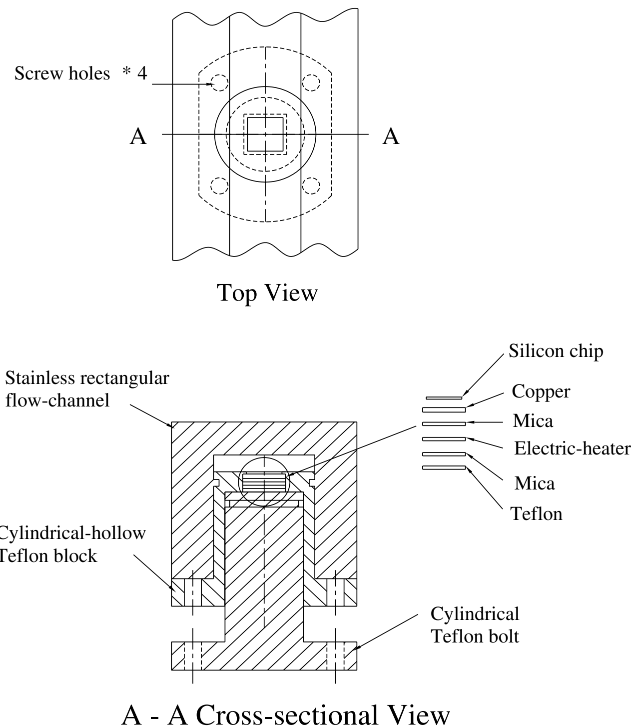

Fig. 2. Schematic of silicon chip module.

Pin-finned 200 surface

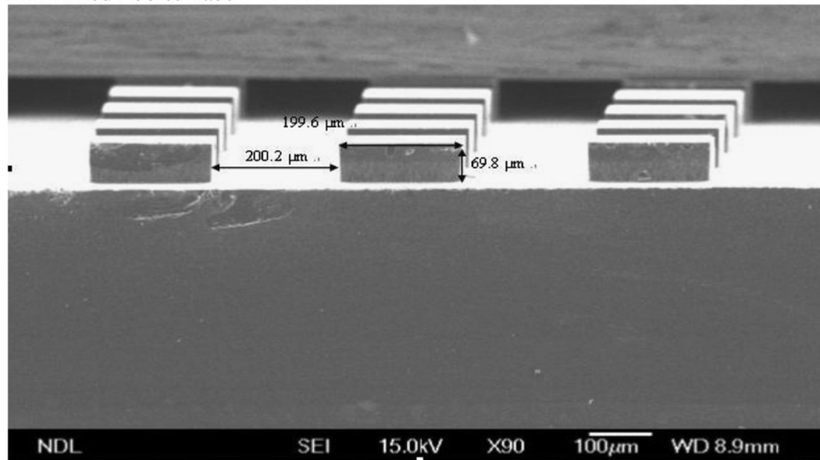

Width × Length × Height: about 200 μm × 200 μm × 70 μm, Space: 200 μm

Pin-finned 100 surface

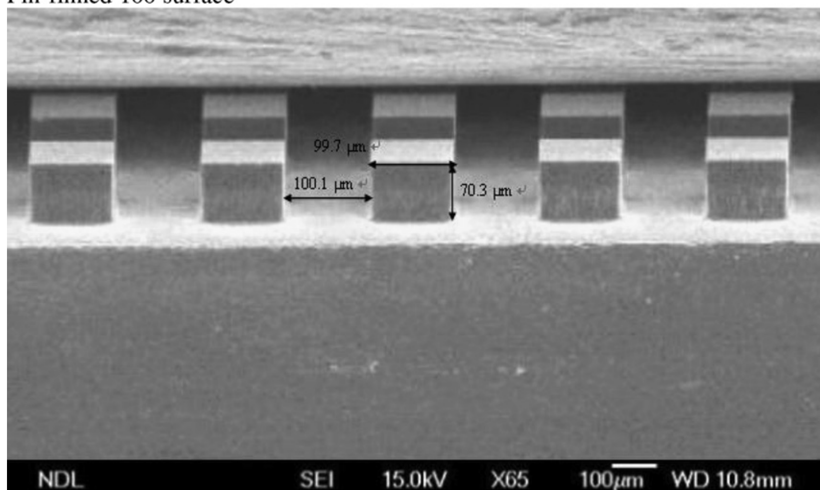

Width × Length × Height: about 100 μm × 100 μm × 70 μm, Space: 100 μm

Fig. 3. Photographs of micro-pin-fins on the silicon chips taken by SEM.

pin-fins on the chips taken by the electronic microscope are shown in Fig. 3.

2.4. Hot-water loop

In order to maintain the coolant FC-72 at the preset temperature at the test section inlet, a hot-water loop is used to preheat the coolant before it arrives at the test section inlet. The hot-water loop includes a thermostat with a 20-liter hot-water container, a 2-kW heater and a 0.5-hp water pump which can drive the water at a specified flow rate to the pre-heater. Besides, a bypass valve in the loop can further adjust the water flow rate. The connecting pipe between the pre-heater and test section is thermally insulated with a 5-cm thick polyethylene layer.

2.5. Cold-water loop

The cold-water loop is designed for condensing the liquid–vapor mixture of FC-72 from the test section. The maximum cooling capacity of the thermostat is 2000 Kcal/h. The cold water at a specific flow rate is driven by a 0.5-hp pump to the condenser and a bypass loop is provided to adjust the flow rate. By adjusting the temperature and flow rate of the cold water, the bulk temperature of FC-72 in the condenser can be controlled at a preset level.

2.6. DC power supply

A 30V-3A DC power supply delivers the required electric current to the electric heater. A Yokogawa data logger is used to measure the DC voltage across and DC current passing through the heater with an accuracy of ±1%. Thus the power input to the heater can be calculated.

2.7. Data acquisition

The data acquisition system employed to acquire and process the data from various transducers is a 20-channel

data logger (YOKOGAWA DA-100) along with a personal computer. The voltage signals from the thermocouples, pressure transducers, and volume flow-meters are converted to the temperature, pressure, and volume flow rate by the internal calibration equations in the computer and are displayed on the screen simultaneously.

2.8. Optical measurement technique

The photographic apparatus consists of a high speed digital video camera (IDT High-speed CMOS Digital Camera), a micro-lens (Optem Zoom 160), a three-dimensional positioning mechanism, and a personal computer. The high-speed camera can take photographs up to 143,307 frames/s. Here, a recording rate of 5000 frames/s is adopted to obtain the images of the bubble ebullition processes. The positioning mechanism is used to hold the camera at the required accurate position. The data for the bubble characteristics are collected in the regions near the geometric center of the chip surface. After the flow reaches a statistically steady state, we start recording the boiling activity. The high speed camera stores the images which are later downloaded to a personal computer. Then, the mean bubble departure diameter and frequency and active nucleation site density are calculated by viewing more than 500 frames for each case. In order to achieve the highest possible resolution and to eliminate errors in calibration, the camera lens is fixed at a constant focal length, resulting in a fixed viewing area. Typically, a total of over 150 bubble diameter measurements is used to construct the present data. The bubble departure frequency is measured by counting the total number of bubbles that emerge from the targeted heating surface area during a period of a second.

2.9. Experimental procedures

Before conducting the experiments, the liquid FC-72 is degassed and then filled into the coolant receiver. Besides, the non-condensable gases in the coolant loop is evacuated. In each test, we first turn on the pump controller and set the inverter frequency to the required rotation rate of the AC motor to regulate the FC-72 flow rate to a preset level. Then the temperature and flow rate of the hot-water loop are selected so that the FC-72 temperature at the test section inlet can be maintained at a preset level. The imposed heat flux to the coolant in the test section is adjusted by varying the electric current delivered from the DC power supply. In addition, the current delivered to and voltage drop across the heater are measured. Temperature and flow rate of the cold water in the cold-water loop can be adjusted to condense the liquid–vapor mixture of FC-72 from the test section. Next, we regulate the FC-72 pressure at the test section inlet by adjusting the gate valve locating right after the test section exit. Meanwhile we use the bypass valve to further adjust the coolant flow rate to the required level. All measurements proceed when the experimental system has reached statistically stable state. Finally, all the data channels are scanned every 1 s for a period of 30 s.

3. Data reduction

At first, the total heat loss of the test section is evaluated from the difference between the total power input Q_t to the silicon chip and the effective power input Q_e to the coolant flow over the chip. The total power input can be calculated from the measured voltage drop across and electric current passing through the electric-heater, $Q_t = V \cdot I$. The effective power input from the chip to the coolant is directly evaluated by assuming the 1-D heat conduction across the copper and mica plates sandwiched between the silicon chip and electric heater by neglecting the heat loss from the side-walls of the cooper and mica plates,

$$Q_e = \frac{\Delta T_{c,h}}{R_{c,h}} \tag{1}$$

where $\Delta T_{c,h} = T_{heater} - T'_{chip}$ is the temperature difference between the upper surface of the heater and lower surface of the chip. And $R_{c,h}$ is the total thermal resistance from the upper heater surface to the lower chip surface including the resistances of the copper and mica plates. Here T'_{chip} is the average measured temperature at the thermocouple locations on the lower surface of the chip. The imposed heat flux at the chip surface is defined as

$$q'' = Q_e/A_{chip} \tag{2}$$

where A_{chip} is the surface area of the bare chip. The relative heat loss from the test section is defined as

$$\varepsilon = (Q_t - Q_e)/Q_t \tag{3}$$

In the present experiments the relative heat loss ε is found to be less than 5% for all cases.

The average single-phase liquid convection heat transfer coefficient over the chip is defined as

$$h_l = \frac{Q_e}{A_{chip} \cdot (T_{chip} - T_{in})} \tag{4}$$

where T_{in} is the coolant temperature at the inlet of the test section and T_{chip} is the average temperature of the upper surface of the chip which is estimated from the measured data for the lower surface of the chip by accounting for the 1-D heat conduction across the chip.

On the other hand, the average two-phase heat transfer coefficient for the coolant flow over the silicon chip is defined as

$$h_r = \frac{Q_e}{A_{chip} \cdot (T_{chip} - T_{sat})} \tag{5}$$

where T_{sat} is the saturated temperature of the coolant FC-72.

Uncertainties of the single-phase liquid convection and flow boiling heat transfer coefficients and other parameters are estimated by the procedures proposed by Kline and

Table 1
Summary of the uncertainty analysis

Parameter	Uncertainty
Rectangular channel geometry	
Length, width and thickness (%)	±0.5%
Area (%)	±1.0%
Parameter measurement	
Temperature, T (°C)	±0.2
Temperature difference, ΔT (°C)	±0.3
System pressure, P (kPa)	±2
Mass flux of coolant, G (%)	±2
Single-phase heat transfer in rectangular channel	
Imposed heat flux, q'' (%)	±4.2
Heat transfer coefficient, h_l (%)	±12.3
Saturated flow boiling heat transfer in rectangular channel	
Imposed heat flux, q'' (%)	±4.2
Heat transfer coefficient, h_r (%)	±12.3

McClintock [23]. The detailed results from this uncertainty analysis are summarized in Table 1.

4. Results and discussion

The present experiments are carried out for the FC-72 mass flux G varying from 287 kg/m^{2}s to 431 kg/m^{2}s and the imposed heat flux q'' from 0.1 W/cm^2 to 10 W/cm^2. Besides, three silicon chips with the smooth, pin-finned 200 and pin-finned 100 surfaces are tested. The coolant is at a pressure slightly lower than 1 atm with $T_{sat} = 54.3$ °C. Selected data are presented here to illustrate the effects of the coolant mass flux, imposed heat flux, and surface micro-structures on the saturated flow boiling heat transfer performance and associated bubble characteristics. The heat transfer performance is presented in terms of the boiling curves and boiling heat transfer coefficients.

4.1. Single-phase liquid convective heat transfer

Before beginning the boiling experiments, single-phase convective heat transfer tests are conducted for liquid FC-72. The measured mean single-phase liquid convection heat transfer coefficients for the chip with a smooth surface are compared with the correlation proposed by Gersey and Mudawar [1] for FC-72. Their correlation is

$$Nu_l = 0.362 \cdot Re_l^{0.614} \cdot Pr^{1/3} \tag{6}$$

where $Re_l = \frac{G \cdot L}{\mu_l}$ and $h_l = \frac{k_l}{L} \cdot Nu_l$.

The comparison is shown in Fig. 4a for the dimensional heat transfer coefficients. The results indicate that our data are in a reasonable agreement with their correlation. Then the present data for the chips with the pin-finned surfaces are given in Fig. 4b. Note that a significant enhancement in the liquid convection heat transfer can be obtained by adding the micro-pin-fins to the chip surface. The enhancement is more pronounced at a higher flow rate (Reynolds number). Besides, the chip surface with the smaller and denser fins shows a better heat transfer performance. The present data for the liquid convection from the pin-finned surfaces can be correlated as

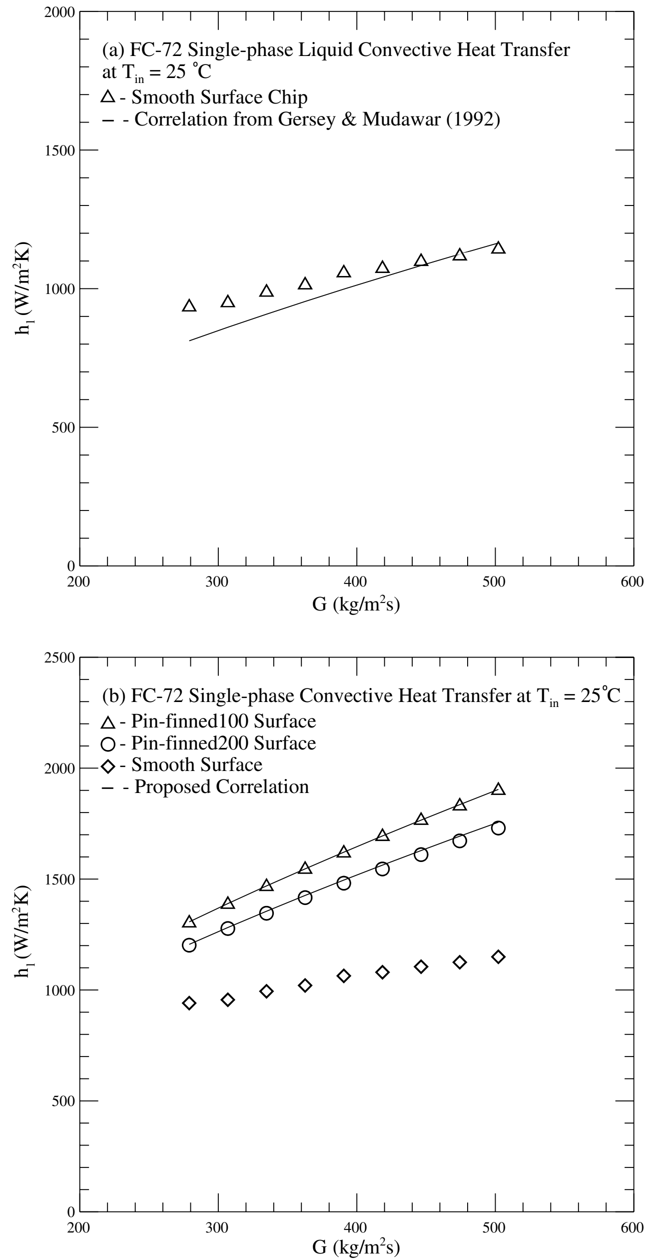

Fig. 4. Comparison of the present single-phase liquid convection heat transfer coefficient for the chip with (a) a smooth surface with the correlation of Gersey and Mudawar [1] and (b) micro-pin-fins with the proposed correlation.

$$Nu_l = 0.33 \cdot Re_l^{0.64} \cdot Pr^{1/3} \cdot F_{sp} \tag{7}$$

with the factor F_{sp} accounting for the geometry effects of the fins and it can be correlated as

$$F_{sp} = \left(\frac{S_f}{H}\right)^{-0.15} \left(\frac{H - B_f}{W_f}\right)^{-0.06} \left(\frac{NA_f}{A_{chip}}\right)^{0.04} \tag{8}$$

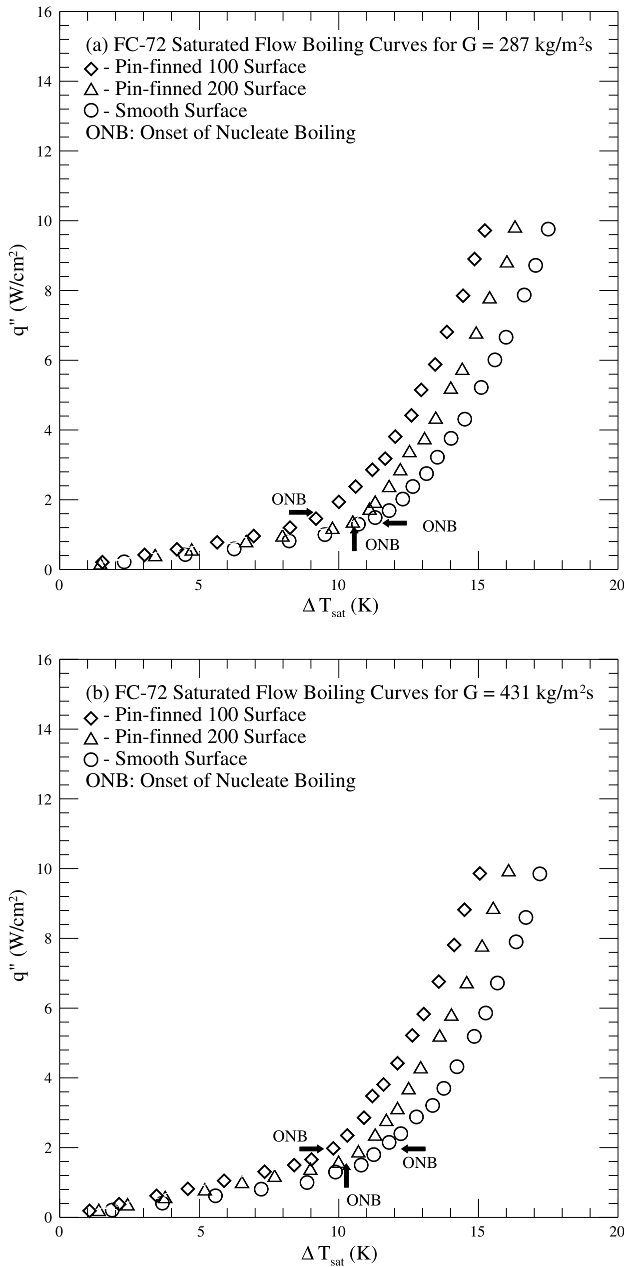

Fig. 5. Boiling curves for various micro-structures of chip surface at (a) $G = 287\ \text{kg/m}^2\ \text{s}$ and (b) $G = 431\ \text{kg/m}^2\ \text{s}$.

Here S_f is the pitch of the fin array, H the rectangular channel height, B_f the fin height, W_f the fin width, N the total number of pin-fins, and A_f is the surface area of a single fin. It should be mentioned that all the working fluid properties used in reducing the data for Fig. 4 and Eqs. (6)–(8) are evaluated at T_{in}.

4.2. Saturated flow boiling curves

The effects of the coolant mass flux and surface microstructure of the heated silicon chip on the boiling curves are shown in Fig. 5. Note that for given G and surface structure the chip surface temperature increases gradually with the imposed heat flux at a low q'' from the saturated temperature of the coolant to a certain value just exceeding T_{sat} and no bubble nucleation is observed. The heat transfer in this region is completely due to the single-phase forced convection. With the continuing increase in q'', bubbles begin to appear on the surface and the boiling curve is characterized by a sharp increase in the surface heat flux for a small rise in the temperature of the chip surface. We have onset of nucleate boiling (ONB) in the flow. The reason causing the transition in the boiling curve is due to a significant increase in the surface heat transfer by the boiling processes. It is also noted by comparing the data in Figs. 5a and b that beyond ONB the coolant mass flux has rather slight effects on the boiling curves, sug-

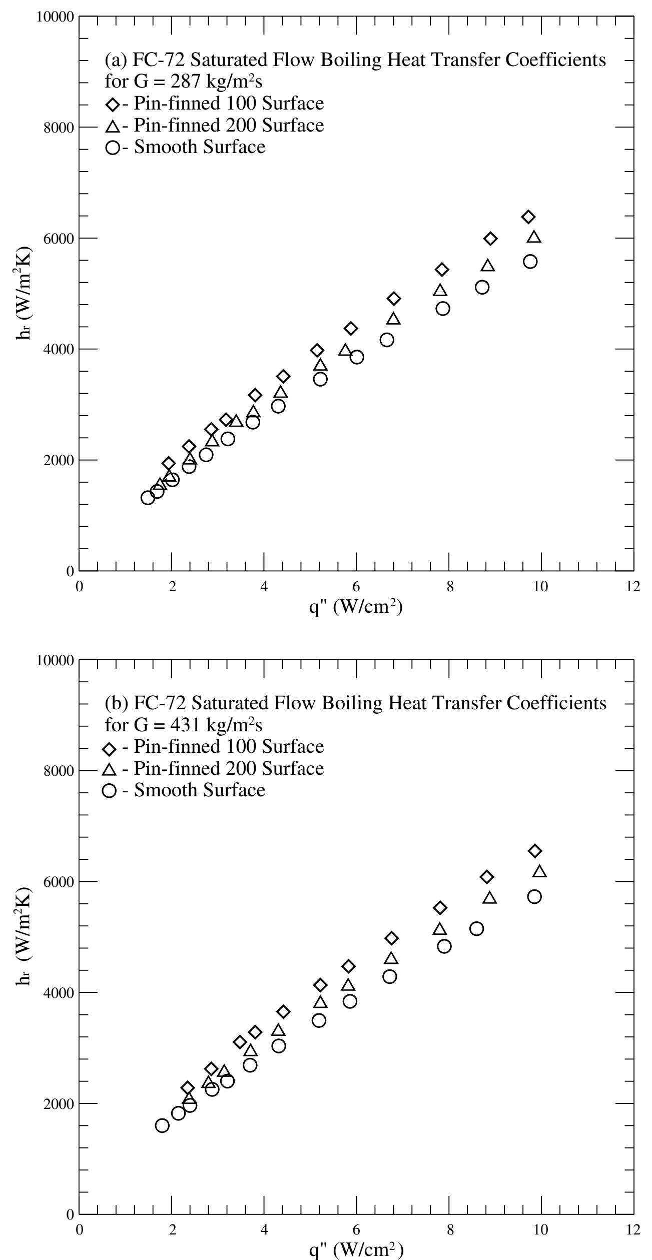

Fig. 6. Saturated flow boiling heat transfer coefficients for various micro-structures of chip surface at (a) $G = 287\ \text{kg/m}^2\ \text{s}$ and (b) $G = 431\ \text{kg/m}^2\ \text{s}$.

gesting that the surface heat transfer is mainly dominated by the fully developed nucleate boiling. Besides, at a higher G the required heat flux for ONB is higher and this implies that more energy is needed for the vapor to nucleate from the wall since the residence time of the coolant on the chip is shorter. The results in Fig. 5 further indicate that for given G in both the single-phase and nucleate boiling regions at the same wall superheat the chip surface heat flux is highest for the pin-finned 100 surface and lowest for the smooth surface, showing that using the micro-pin-finned structure can effectively enhance the single-phase and flow boiling heat transfer from the chip surface. The large increase in the total surface area by adding the micro-pin-fins is indeed beneficial for the single- and two-phase heat transfer. Moreover, the wall superheat required for the boiling inception is substantially lower for the pin-finned 100 surface. This is attributed to the increase in the density of the active nucleation sites by the surface micro-structures. Particularly, in the corner region of the pin-fins the bubbles are found to appear at lower ΔT_{sat}.

4.3. Saturated flow boiling heat transfer coefficient

We continue to explore how the saturated flow boiling heat transfer coefficient h_r is affected by the FC-72 mass flux and surface micro-structure on the silicon chips. The data presented in Fig. 6 for the variations of h_r with the surface heat flux reveal that for the three tested surfaces the coolant mass flux shows negligible influences on h_r. However, for a given coolant mass flux G the boiling heat transfer coefficient increases substantially with the imposed heat flux. Moreover, adding the surface micro-structures in the form of micro-pin-fins to the silicon chip produces some positive effects on the boiling heat transfer coefficient at high imposed heat flux. This is due to the fact that the boiling heat transfer performance can be raised effectively by the addition of active nucleation sites from the pin-fin structures. Besides, the heat transfer is further enhanced by a serpentine motion of liquid between adjacent rows of pin-fins, which in turn enhances turbulent mixing [16,17]. Furthermore, development of multiple thermal entry regions at the top surfaces of individual pin-fins is beneficial.

4.4. Bubble characteristics

To elucidate the saturated flow boiling heat transfer characteristics presented above, the bubble characteristics obtained from the present flow visualization are examined in the following. At first, the top views of the boiling flow for various coolant mass fluxes and imposed heat fluxes are shown in Fig. 7. Bubbles begin to appear as the chip surface temperature exceeds the incipient boiling superheat. In the beginning, tiny bubbles are seen on the active nucle-

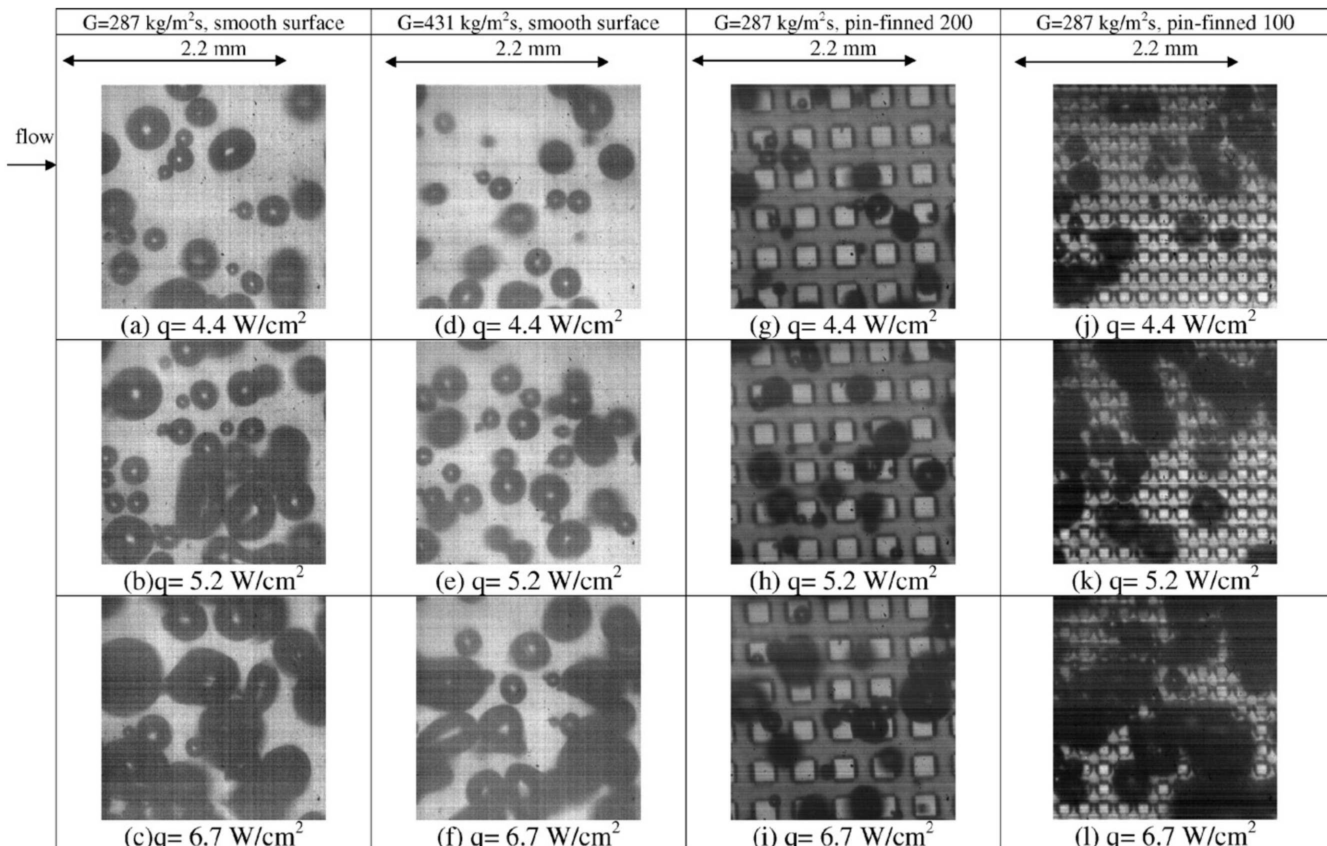

Fig. 7. Photos of bubbles in the saturated flow boiling of FC-72 for various imposed heat fluxes, mass fluxes and chip surfaces.

ation sites. The bubbles grow and then detach from the chip surface. As q'' increases, more bubbles are generated at more active nucleation sites and more bubbles detach from the chip surface. Besides, the detached bubbles tend to merge into larger bubbles, which occurs more frequently at a higher q''. Note that the large bubbles become distorted and elongated when moving downstream. To quantify the bubble characteristics, the data for the mean bubble departure diameter and frequency and active nucleation site density are given in Figs. 8–13.

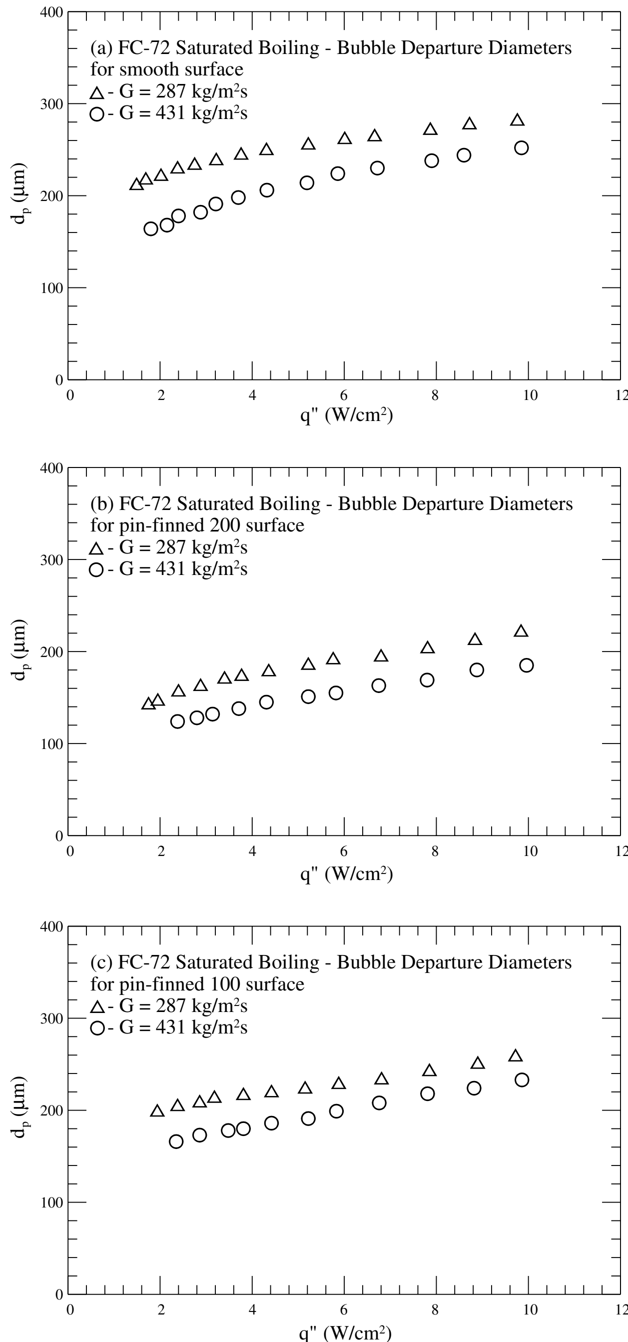

Fig. 8. Mean bubble departure diameters for various coolant mass fluxes for the chips with (a) smooth surface, (b) pin-finned 200 surface and (c) pin-finned 100 surface.

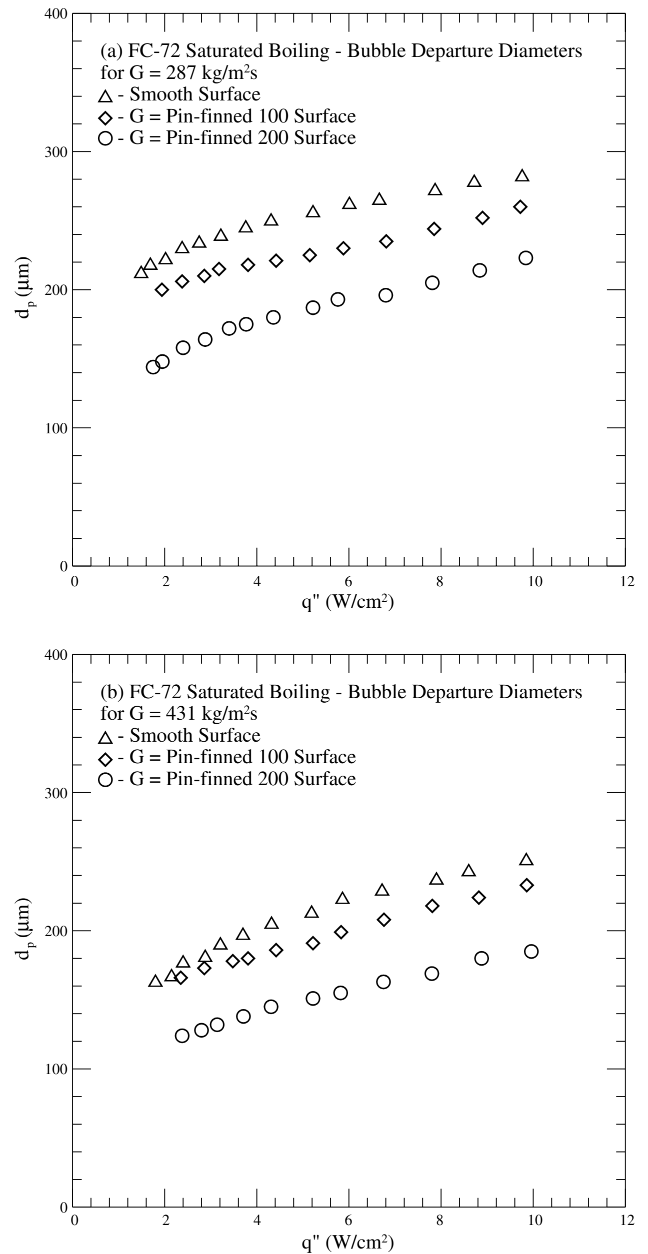

Fig. 9. Mean bubble departure diameters for various micro-structures of chip surface at (a) $G = 287\ \text{kg/m}^2\ \text{s}$ and (b) $G = 431\ \text{kg/m}^2\ \text{s}$.

The results in Fig. 8 indicate that the mean size of the bubbles departing from the chips can be reduced substantially by increasing the coolant mass flux. It is ascribed to the fact that the coolant at a higher mass flux and hence at a higher speed tends to sweep the bubbles more quickly away from the heating surface. Besides, the addition of the micro-pin-fins to the chips is found to cause a significantly earlier departure of the bubbles and results in a smaller d_p (Fig. 9). The partially accelerated coolant flow between the fins can increase the drag force on the bubbles and sweep them away from the finned surface earlier. Note that for a given G the mean bubble departure diameter for the pin-finned 100 surface is larger than that for the pin-finned 200 surface. This due to the fact that the spaces between the

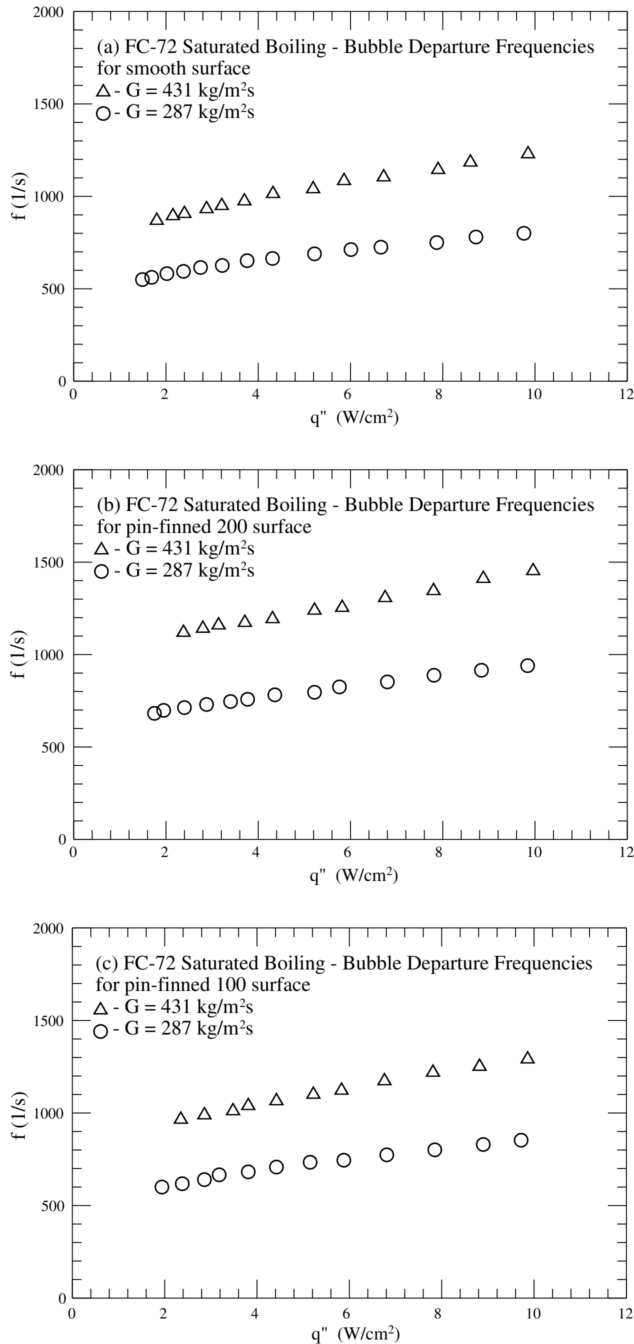

Fig. 10. Mean bubble departure frequencies for various coolant mass fluxes for the chips with (a) smooth surface, (b) pin-finned 200 surface and (c) pin-finned 100 surface.

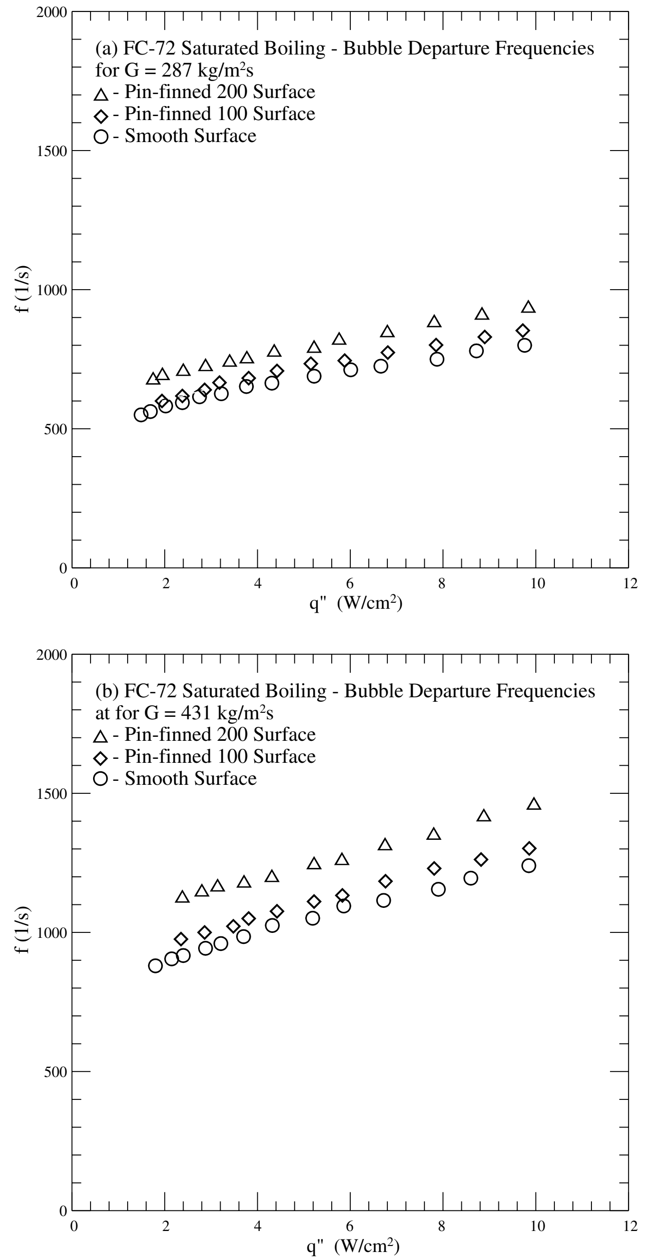

Fig. 11. Mean bubble departure frequencies for various micro-structures of chip surface at (a) $G = 287$ kg/m^2 s and (b) $G = 431$ kg/m^2 s.

adjacent fins for the pin-finned 100 surface are so small and the bubbles already contact the sides of the fins before departure. Therefore, the bubbles grow for a longer period of time before departure. Longer bubble growth time causes the growing bubble to keep absorbing energy from the heated surface for a longer period of time and results in a larger d_p.

Next, the data given in Fig. 10 manifest that raising the coolant mass flux can significantly augment the mean bubble departure frequency f. The increase of f with G is ascribed again to the higher drag on the bubbles still attaching to the chip surface by the liquid coolant moving at a higher speed for a higher G. This, in turn, causes an earlier departure of the bubbles from the surface, resulting in a higher f. It is also observed that the mean bubble departure frequency increases noticeably with q''. Finally, the data given in Fig. 11 indicate that f can be enhanced effectively by using the pin-finned surface and the effect is slightly larger on the pin-finned 200 surface than the pin-finned 100 surface.

Attention is turned to the data for the mean active nucleation site density N_{ac} shown in Figs. 12 and 13. N_{ac} is calculated based on the surface area of a bare chip. Fig. 12 manifests that an increase in the coolant mass flux

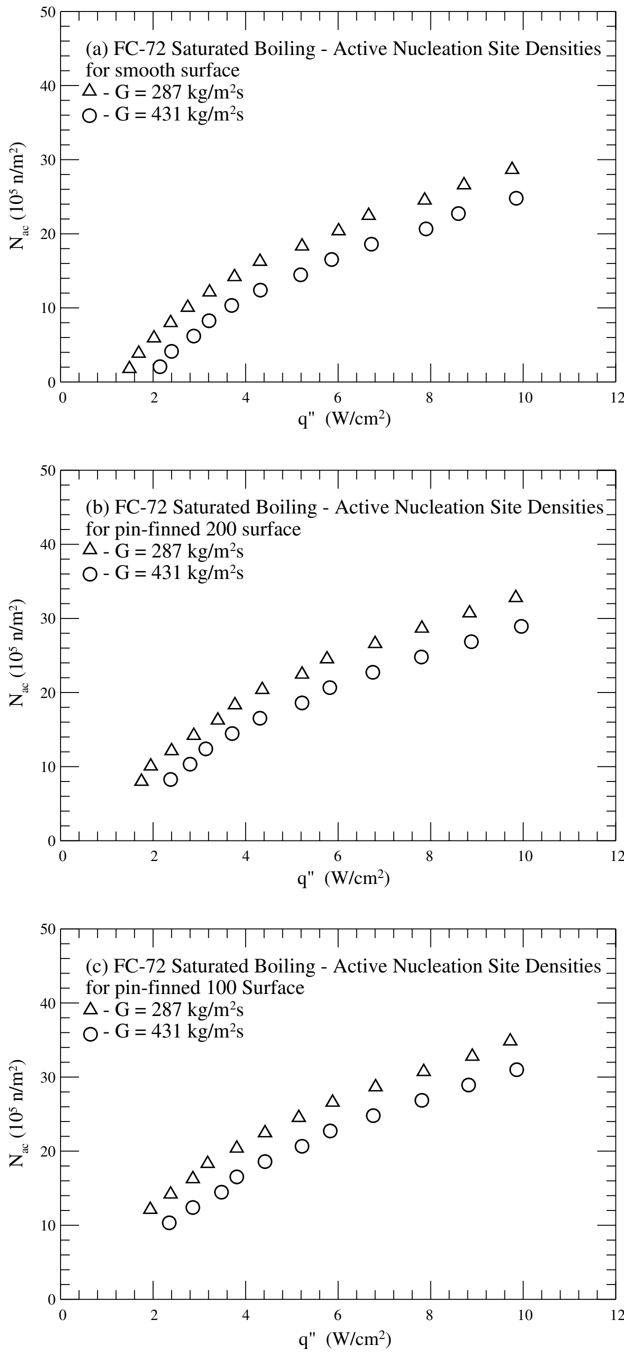

Fig. 12. Mean active nucleation site densities for various coolant mass fluxes for the chips with (a) smooth surface, (b) pin-finned 200 surface and (c) pin-finned 100 surface.

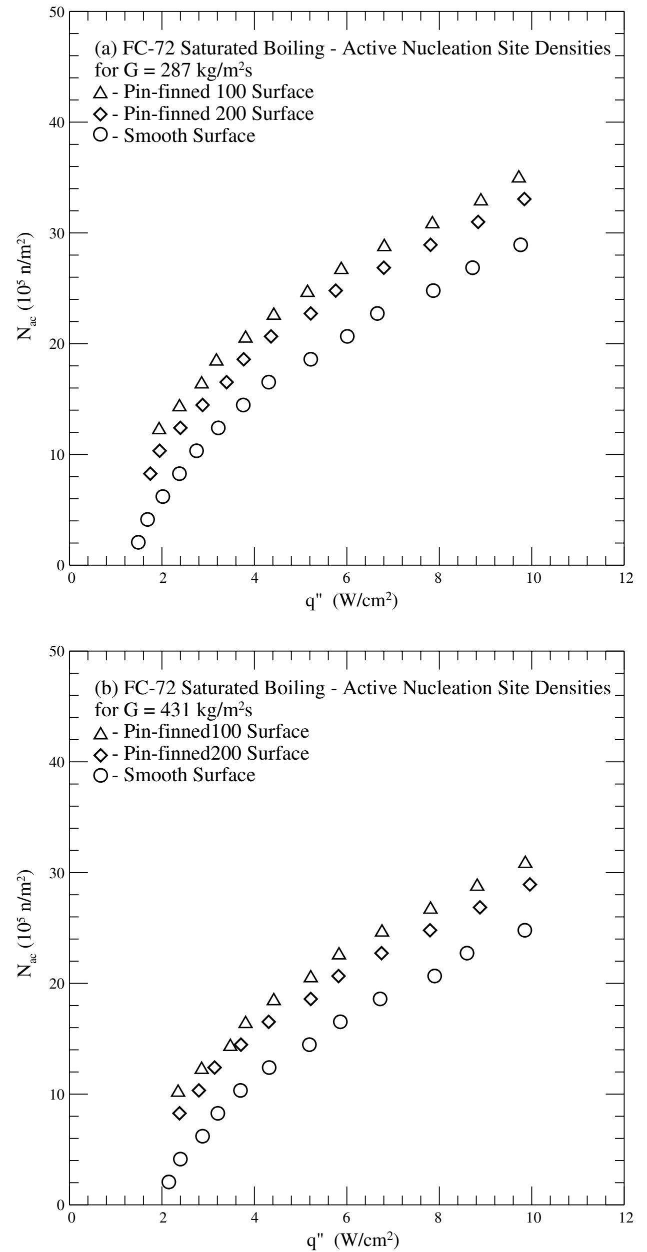

Fig. 13. Mean active nucleation site densities for various micro-structures of chip surface at (a) $G = 287$ kg/m^{2}s and (b) $G = 431$ kg/m^{2}s.

results in somewhat lower N_{ac} for the three surfaces. This directly relates to the fact that the higher imposed heat flux is needed for the boiling inception at a higher G, as already discussed in the previous section. Finally, it is noted from Fig. 13 that adding the micro-pin-fins to the chip surface can effectively increase the active nucleation sites. This is due to the increase in the surface area of micro-pin-fins. Moreover, N_{ac} on the pin-finned 100 surface is slightly higher than the pin-finned 200 surface.

4.5. Correlation equations

Based on the present experimental data, empirical correlations for the bubble characteristics and heat transfer coefficient in the saturated flow boiling of FC-72 on the heated silicon chip flush-mounted on the bottom of the rectangular channel are proposed.

First, the data for the average bubble departure diameter can be correlated as

$$\overline{d_p} \equiv \frac{d_p}{\sqrt{\sigma/g \cdot \Delta\rho}} = \frac{0.25 \cdot (\rho_l/\rho_v)^{0.48} \cdot Bo^{0.21}}{Re_l^{0.08}} \quad \text{for the smooth surface} \quad (9)$$

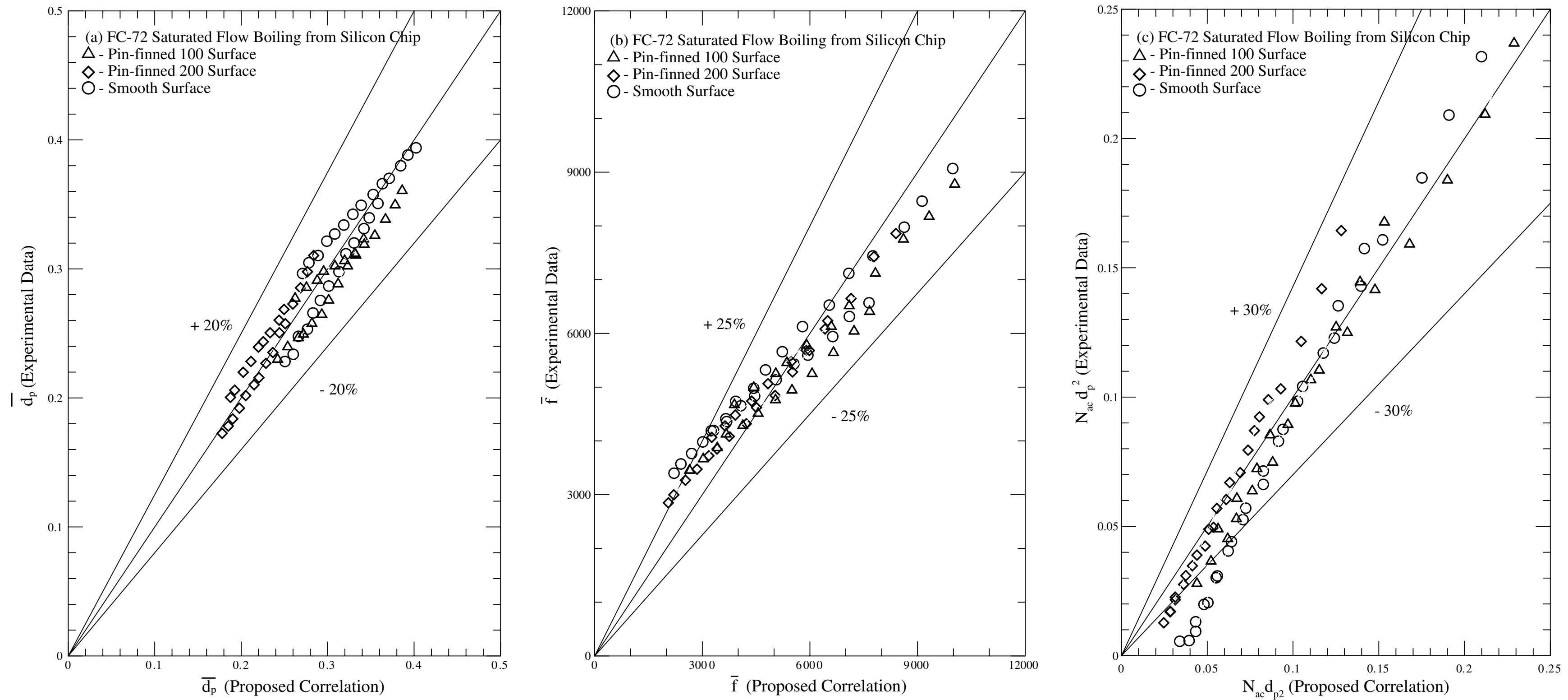

Fig. 14. Comparison of the measured data with the proposed correlations in the saturated flow boiling of FC-72 for (a) mean bubble departure diameter, (b) mean bubble departure frequency and (c) mean active nucleation site density.

and

$$\overline{d_p} \equiv \frac{d_p}{\sqrt{\sigma/g \cdot \Delta\rho}} = \frac{0.15 \cdot (\rho_l/\rho_v)^{0.46} \cdot Bo^{0.24} \cdot F_{d,sat}}{Re_l^{0.07}}$$
for the pin-finned surfaces (10)

with the fin-geometry factor $F_{d,sat}$ correlated as

$$F_{d,sat} = \left(\frac{S_f}{H}\right)^{-0.12} \left(\frac{H - B_f}{W_f}\right)^{0.05} \left(\frac{N \cdot A_f}{A_{chip}}\right)^{0.42} \quad (11)$$

Fig. 14a shows that the present data for $\overline{d_p}$ fall within ±20% of the correlations given above. In addition, the data for the mean bubble departure frequency can be correlated as

$$\bar{f} \equiv \frac{f \cdot d_p}{\mu_l/\rho_l \cdot D_h} = 0.65 Re_l^{1.3} \cdot Pr^{0.7} \cdot Bo^{0.66} \quad \text{for the smooth surface} \quad (12)$$

and

$$\bar{f} \equiv \frac{f \cdot d_p}{\mu_l/\rho_l \cdot D_h} = 0.21 Re_l^{1.3} \cdot Pr^{0.72} \cdot Bo^{0.66} \cdot F_{f,sat}$$
for the pin-finned surfaces (13)

with the fin-geometry factor $F_{f,sat}$ correlated as

$$F_{f,sat} = \left(\frac{S_f}{H}\right)^{0.12} \left(\frac{H - B_f}{W_f}\right)^{0.4} \left(\frac{N \cdot A_f}{A_s}\right)^{-0.02} \quad (14)$$

Fig. 14b reveals that most of the present data for $f \cdot d_p$ fall within ±25% the above two equations. Moreover, correlations for the mean active nucleation site density are proposed as

$$N_{ac} \cdot d_p^2 = 75 \cdot Bo^{0.84} \cdot Re_l^{-0.15} \quad \text{for the smooth surface} \quad (15)$$

and

$$N_{ac} \cdot d_p^2 = 72 \cdot Bo^{0.87} \cdot Re_l^{-0.15} \cdot F_{n,sat} \quad \text{for the pin-finned surfaces} \quad (16)$$

with the factor $F_{n,sat}$ correlated as

$$F_{n,sat} = \left(\frac{S_f}{H}\right)^{-0.15} \left(\frac{H - B_f}{W_f}\right)^{-0.06} \left(\frac{N \cdot A_f}{A_s}\right)^{1.15} \quad (17)$$

Note that $F_{d,sat}$, $F_{f,sat}$ and $F_{n,sat}$ are the dimensionless factors to include the fin-geometry effects on the bubble characteristics. The comparison given in Fig. 14c shows that more than 85% of the present experimental data for N_{ac} fall within ±30% of the above correlations.

Finally, the heat flux to the boiling flow q'' is considered to be composed of two parts: one resulting from the bubble nucleation q''_b and another due to the single-phase forced convection q''_c. Thus

$$q'' = q''_b + q''_c \quad (18)$$

Here q''_b can be estimated from the above correlations for the bubble characteristics as

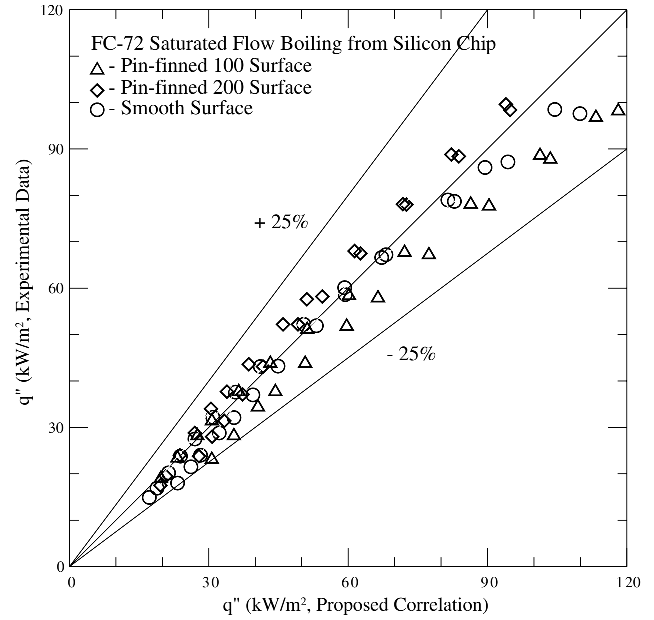

Fig. 15. Comparison of the measured heat transfer data with the proposed correlation in the saturated flow boiling of FC-72.

$$q''_b = \rho_v \cdot V_b \cdot f \cdot N_{ac} \cdot i_{lv} \quad (19)$$

where ρ_v is the vapor density, V_b is the mean volume of the departing bubble defined as $\frac{4\pi}{3}\left(\frac{d_p}{2}\right)^3$, and i_{lv} is the enthalpy of vaporization. Besides, q''_c can be estimated from the single-phase liquid convection as

$$q''_c = E \cdot h_l \cdot \Delta T_{sat} \quad (20)$$

where E is an enhancement factor to account for the agitating motion of the bubbles which can enhance the single-phase heat transfer. From the present data, E can be empirically correlated as

$$E = 4.5 \cdot N_{conf}^{0.5} \cdot Fr_l^{0.15} \cdot (1 + 280 \cdot Bo)^{1.8}$$
for the smooth surface (21)

and

$$E = 2.8 \cdot N_{conf}^{0.5} \cdot Fr_l^{0.13} \cdot (1 + 270 \cdot Bo)^{1.8} \cdot F_{E,sat}$$
for the pin-finned surfaces (22)

with the fin-geometry factor $F_{E,sat}$ correlated as

$$F_{E,sat} = \left(\frac{S_f}{H}\right)^{-0.16} \left(\frac{H - B_f}{W_f}\right)^{-0.1} \left(\frac{N \cdot A_f}{A_s}\right)^{0.02} \quad (23)$$

The comparison shown in Fig. 15 indicate that nearly all the present heat transfer data fall within ±25% of the above correlations with an average deviation of 8.9%.

5. Concluding remarks

An experiment has been carried out to investigate saturated flow boiling of FC-72 on a heated micro-pin-finned silicon chip flush-mounted on the bottom of a rectangular channel. The effects of the imposed heat flux, coolant mass

flux and surface structure on the measured data have been examined in detail. Furthermore, empirical equations to correlate the measured data are proposed. The major results obtained here can be summarized as follows:

(1) The boiling incipience heat flux is higher at a higher coolant mass flux.
(2) The coolant mass flux shows little influence on h_r. Besides, increasing the imposed heat flux significantly promotes boiling heat transfer. Moreover, addition of the micro-pin-fins to the chips is also beneficial.
(3) The mean bubble departure diameter is reduced at increasing mass flux but the departing bubbles are significantly larger at a higher imposed heat flux. The bubbles departing from the heated surfaces are found to be somewhat smaller for the pin-finned surfaces.
(4) The bubble departure frequency increases with the coolant mass flux and imposed heat flux. Besides, higher bubble departure frequency is found on the pin-finned surfaces.
(5) The active nucleation site density decreases at increasing coolant mass flux. However, an opposite trend results for an increase in the imposed heat flux and for the addition of the micro-pin-fin structures to the chip surfaces.

Acknowledgement

The financial support of this study by the engineering division of National Science Council of Taiwan, ROC through the contract NSC 93-2212-E-009-005 is greatly appreciated.

References

[1] C.O. Gersey, I. Mudawar, Effects of orientation on critical heat flux from chip arrays during flow boiling, Trans. ASME J. Electr. Pack. 114 (1992) 290–299.
[2] T.C. Willingham, I. Mudawar, Forced-convection boiling and critical heat flux from a linear array of discrete heat sources, Int. J. Heat Mass Transfer 35 (1992) 2879–2890.
[3] T.J. Heindel, S. Ramadhyani, F.P. Incropera, Liquid immersion cooling of a longitudinal array of discrete heat sources in protruding substrates: II – forced convection boiling, Trans. ASME J. Electr. Pack. 114 (1992) 63–70.
[4] W.R. McGills, V.P. Carey, B.D. Strom, Geometry effects on critical heat flux for subcooled convective boiling from an array of heated elements, Trans. ASME J. Heat Transfer 113 (1991) 463–471.
[5] C.P. Tso, K.W. Tou, G.P. Xu, Flow boiling critical heat flux of FC-72 from flush-mounted and protruded simulated chips in a vertical rectangular channel, Int. J. Multiphase Flow 26 (2000) 351–365.
[6] K.R. Samant, T.W. Simon, Heat transfer from a small heated region to R-113 and FC-72, Trans. ASME J. Heat Transfer 111 (1989) 1053–1059.
[7] Y. Ma, J.N. Chung, A study of bubble dynamics in reduced gravity forced-convection boiling, Int. J. Heat Mass Transfer 44 (2001) 399–415.
[8] R. Situ, Y. Mi, M. Ishii, M. Mori, Photographic study of bubble behavior in forced convection subcooled boiling, Int. J. Heat Mass Transfer 47 (2004) 3659–3667.
[9] C.P. Yin, Y.Y. Yan, T.F. Lin, B.C. Yang, Subcooled flow boiling heat transfer of R-134a and bubble characteristics in a horizontal annular duct, Int. J. Heat Mass Transfer 43 (2000) 1885–1896.
[10] C. Bang, Won-Pil Baek, S.H. Chang, A digital photographic study on nucleate boiling in subcooled flow for water and refrigerant 134A fluids, in: Proceedings of ICONE10 10th International Conference on Nuclear Engineering Arlington, VA, April 14–18, 2002.
[11] S.H. Chang, I.C. Bang, Won-Pil Baek, A photographic study on the near-wall bubble behavier in subcooled flow boiling, Int. J. Therm. Sci. 41 (2002) 609–618.
[12] C. Bang, S.H. Chang, Won-Pil Baek, Visualization of the subcooled flow boiling of R-134a in a vertical rectangular channel with an electrically heated wall, Int. J. Heat Mass Transfer 47 (2004) 4349–4363.
[13] R. Maurus, V. Ilchenko, T. Sattelmayer, Study of the bubble characteristics and the local void fraction in subcooled flow boiling using digital imaging and analyzing techniques, Exp. Therm. Fluid Sci. 26 (2002) 147–155.
[14] R. Maurus, V. Ilchenko, T. Sattelmayer, Automated high-speed video analysis of the bubble dynamics in subcooled flow boiling, Int. J. Heat Fluid Flow 25 (2004) 149–158.
[15] G.E. Thorncroft, J.F. Klausner, R. Mei, An experimental investigation of bubble growth and detachment in vertical upflow and downflow boiling, Int. J. Heat Mass Transfer 41 (1998) 3857–3871.
[16] D.E. Maddox, I. Mudawar, Single- and two-phase convective heat transfer from smooth and enhanced microelectronic heat sources in a rectangular channel, Trans. ASME J. Heat Transfer 111 (1989) 1045–1052.
[17] I. Mudawar, D.E. Maddox, Enhancement of critical heat flux from high power microelectronic heat sources in a flow channel, Trans. ASME J. Electr. Pack. 112 (1990) 241–248.
[18] H. Honda, H. Takamastu, J.J. Wei, Enhanced boiling of FC-72 on silicon chips with micro-pin-fins and submicron-scale roughness, Trans. ASME J. Heat Transfer 124 (2002) 383–389.
[19] H. Honda, J.J. Wei, Effects of fin geometry on boiling heat transfer from silicon chips with micro-pin-fins immersed in FC-72, Int. J. Heat Mass Transfer 46 (2003) 4059–4070.
[20] H. Honda, J.J. Wei, Enhanced boiling heat transfer from electronic components by use of surface microstructures, Exp. Therm. Fluid Sci. 28 (2004) 159–169.
[21] C. Ramaswamy, Y. Joshi, W. Nakayama, W.B. Johnson, Effects of varying geometrical parameters on boiling from microfabricated enhanced structures, Trans. ASME J. Heat Transfer 125 (2003) 103–109.
[22] K.N. Rainey, S.M. You, S. Lee, Effect of pressure, subcooling, and dissolved gas on pool boiling heat transfer from microporous, square pin-finned surface in FC-72, Int. J. Heat Mass Transfer 46 (2003) 23–25.
[23] S.J. Kline, F.A. McClintock, Describing uncertainties in single-sample experiments, Mech. Eng. 75 (1953) 3–12.